

# Edge-Preserving Bilateral Filtering for Images Containing Dense Objects in CT

Qiao Yang, Andreas Maier, Nicole Maass, Joachim Hornegger

**Abstract**—In computed tomography (CT), dense objects such as bone, metal implants, and contrast medium, induce cupping and streaking artifacts. To reduce those artifacts, various approaches have a common strategy, which is segmenting datasets into different materials and correcting them separately according to their own physical characteristics. However, in most cases, the severe artifacts hinder the primary segmentation which results in low efficiency of artifact reduction approaches. When taking noise under consideration, the accuracy of segmentation gets even worse. In this work, we applied an edge preserving step based on bilateral filtering between reconstruction and segmentation. A traditional bilateral filter performs noise reduction, and a bilateral edge detector exploits the structural edge information. By incorporating the edge information with noise reduced reconstruction images, a more sophisticated segmentation approach is proposed. Quantitative evaluations of noise reduction and segmentation performance are carried out using simulated and real CT datasets. The results show that our approach can reduce streak artifacts at a primary level, which significantly improves segmentation.

**Index Terms**—Computed Tomography, Beam Hardening Correction, Image Segmentation, Noise Reduction

## I. INTRODUCTION

In CT, the projection images acquired at the detector and consequently, the reconstructed volumes contain quantum noise. The strength of noise varies among different measurements, which leads to inhomogeneous noise in the reconstructed slices. The problem is getting worse when X-rays passing through the scanned objects are attenuated differently due to discrepancies in material type and size, especially in regions containing dense materials like bone, contrast agents, surgical clips, and metal implants. Moreover, the nonlinear attenuation characteristics of polychromatic X-rays causing beam hardening artifacts, together with metal artifacts, result in dark bands or streaks across the images, hiding anatomical structures and pathology, hindering visualization and reducing diagnostic confidence.

To reduce artifacts which are caused by dense objects, various approaches have a common strategy, which is segmenting datasets into different materials and correcting them individually according to their own physical characteristics [1]–[8]. However, due to dense objects inducing severe cupping

Qiao Yang, Andreas Maier and Joachim Hornegger are with the Pattern Recognition Lab, Department of Computer Science, Friedrich-Alexander-Universität Erlangen-Nürnberg, Erlangen, Germany and the Erlangen Graduate School Heterogeneous Imaging Systems. Andreas Maier and Joachim Hornegger are also with the Erlangen Graduate School in Advanced Optical Technologies (SOAT), Friedrich-Alexander-Universität Erlangen-Nürnberg, Erlangen, Germany. Nicole Maass is with Siemens AG, Healthcare Sector, Erlangen, Germany. Email: qiao.yang@cs.fau.de

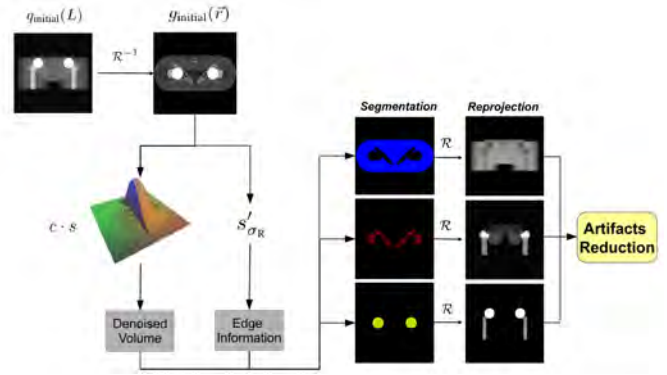


Fig. 1: Flowchart

and streaking artifacts, a more accurate primary segmentation becomes a major challenge, and influences the convergence speed of correction approaches.

In [9], we have proposed an iterative multi-material beam hardening correction scheme. However, when taking noise into consideration, the performance of segmentation is affected significantly. In this paper, we apply an edge preserving step for CT images consisting of dense objects based on bilateral filtering. Its function is not only noise reduction, but also aiding to exploit the structural edge information at the segmentation step in order to achieve a more accurate preliminary segmentation and thus a more efficient artifact reduction afterwards. The algorithm is evaluated using simulation data and real measured CT data. It is shown that our approach can reduce streak artifacts caused by dense objects and also significantly improve the segmentation results from the original reconstructed volumes.

## II. METHODS

Segmentation is always hindered due to image noise and artifacts such as streaks. Therefore, the non-linear edge preserving bilateral filter which can reduce noise and return structural edge information is considered for our case. A brief flowchart is illustrated in Fig. 1.

### A. Bilateral Filtering

Bilateral filtering embodies the idea of a combination of domain and range filtering [10]. From [11], the authors conclude that the bilateral filter in image space has a significant noise reduction while edges are well preserved.

Denote  $\mathbf{r}$  as spatial location on the reconstruction grid, the 3D filtered volume  $\tilde{f}(\mathbf{r})$  is calculated as follows:

$$\tilde{f}(\mathbf{r}) = \frac{1}{n(\mathbf{x})} \sum_{\mathbf{r}'} f(\mathbf{r}') c(\mathbf{r}, \mathbf{r}') s(f(\mathbf{r}), f(\mathbf{r}')), \quad (1)$$

where  $n(\mathbf{x})$  is the sum of all weights and used for normalization:

$$n(\mathbf{x}) = \sum_{\mathbf{r}} c(\mathbf{r}, \mathbf{r}') s(f(\mathbf{r}), f(\mathbf{r}')). \quad (2)$$

The function  $c(\mathbf{r}, \mathbf{r}')$  is the domain filter which takes the geometric distance of the actual voxel  $\mathbf{r}$  and the neighboring voxel  $\mathbf{r}'$  into account:

$$c(\mathbf{r}, \mathbf{r}') = e^{-\frac{\|\mathbf{r}-\mathbf{r}'\|_2^2}{\sigma_b^2}}. \quad (3)$$

The function  $s(f(\mathbf{r}), f(\mathbf{r}'))$  is the range filter, which is the edge-preserving component that compares the gray value of the center pixel to the spatial neighborhood and computes the corresponding weight coefficients depending on the factor  $\sigma_s$ .

$$s(f(\mathbf{r}), f(\mathbf{r}')) = e^{-\frac{(f(\mathbf{r})-f(\mathbf{r}'))^2}{\sigma_s^2}}. \quad (4)$$

### B. Edge Detector

Common edge detection methods like Prewitt, Sobel, Laplacian operators, etc. are normally discontinuous or over-detected. When reconstructed images contain dense objects and suffer from streak artifacts, the performance of those operators are affected. We designed a bilateral edge detector, which applies an inverted range filter on Sobel domain kernel, resulting in the detected edges being emphasized. Hence dissimilar regions in the image are easier to distinguish. The modified range filter can be written as

$$s'_{\sigma_R} = a - e^{-\frac{(f(\mathbf{r})-f(\mathbf{r}'))^2}{\sigma_R^2}} \quad (5)$$

Constant  $a$  is used to avoid zeros, and the value can just be slightly larger than 1.

By application of the edge detector on filtered image  $\tilde{f}(\mathbf{r})$ , the edge image  $\hat{f}_{edge}(\mathbf{r})$  is obtained. Given an optimal threshold  $T$ , the function classifies the pixels into two classes: edge pixels and non-edge pixels:

$$E(x, y) = \begin{cases} 1, & \text{if } \hat{f}_{edge}(\mathbf{r}) \geq T, \text{ edge pixel} \\ 0, & \text{if } \hat{f}_{edge}(\mathbf{r}) < T, \text{ non-edge pixel} \end{cases} \quad (6)$$

Connected edge pixels are merged together and labeled with the same symbol.

### C. Segmentation

Previously, we have proposed a histogram based k-means clustering initialization method for segmentation [12]. We use the obtained centroids from this method as seeds  $S_1, S_2, \dots, S_q$ , and the seeded region growing (SRG) technique is applied. The regions are grown from seed points to adjacent neighborhood pixels. For each step, one additional pixel is incorporated into one of the seed sets. The 8-connected neighborhood is used for pixels' adjacent relationship. If the neighborhood

pixel is in the same cluster with the seeds, and is not an edge point, it will be labeled the same as the seed point. These initial seeds are further replaced by the centroids of the generated regions  $R_1, R_2, \dots, R_q$  by incorporating the additional pixels step by step.

The results of edge detection are integrated to provide more accurate region boundaries. The boundary pixels of each homogeneous region from K-means clustering are first extracted by determining the first and last pixels for each row and column for the same region. These first and last pixels form a boundary for the corresponding region. There are different situations for decision making:

- The boundary pixels, which are detected as both the region boundaries and the structural edges, are classified as the pixels on the final region boundary.
- The region pixels, which are not detected as either region boundaries or edges, should be the pixels inside a region.
- The uncertain pixels which are detected as region boundaries but not as edges, may be the discontinuous points and should be refined on the basis of their neighbors.
- The uncertain pixels which are detected as edges but not as region boundaries, may be the over-detected edge pixels and should be refined on the basis of their neighbors.

As a result, region boundaries are eliminated or modified on the basis of these local edges.

## III. EXPERIMENTS AND RESULTS

Parameter	Jaw Phantom	Hip Prosthesis Phantom	Multi-cylinders
Tube Voltage	120kVp	120kVp	150kVp
SOD	750mm	750mm	1200mm
SDD	800mm	1200mm	1400mm
No. of Projections	600	450	1000
Detector Grid	512×512	512×512	1024×1024
Pixel Size	0.5mm	0.7mm	0.4mm
Volume Grid	512×512×512	512×512×512	400×400×600
Voxel Size	1.0mm	0.3mm	0.5mm
Materials	Soft Tissue, Bone	Soft Tissue, Bone, Ti	Plastic, Al, Fe, Cu

TABLE I: Experimental parameters

In order to quantitatively evaluate the performance on noise reduction and segmentation, polychromatic cone beam CT simulations were carried out using the FORBILD jaw phantom and the hip prosthesis phantom [13]. The projection data was obtained by using the CT simulation software DRASIM (Siemens AG, Forchheim, Germany). Circular 3D raw data was reconstructed using a standard FDK reconstruction algorithm [14]. Furthermore, a real X-ray projected dataset containing four cylinders of different materials was evaluated. The experiments' parameters are listed in Table I.

### A. Noise Reduction

Fig. 2 illustrates the reconstruction results of the jaw phantom. In comparison with a monochromatic reconstruction (Fig. 2a), the dense objects (bone) causing streak artifacts have significant influence on the reconstruction from polychromatic projections with Poisson noise added (Fig. 2b).

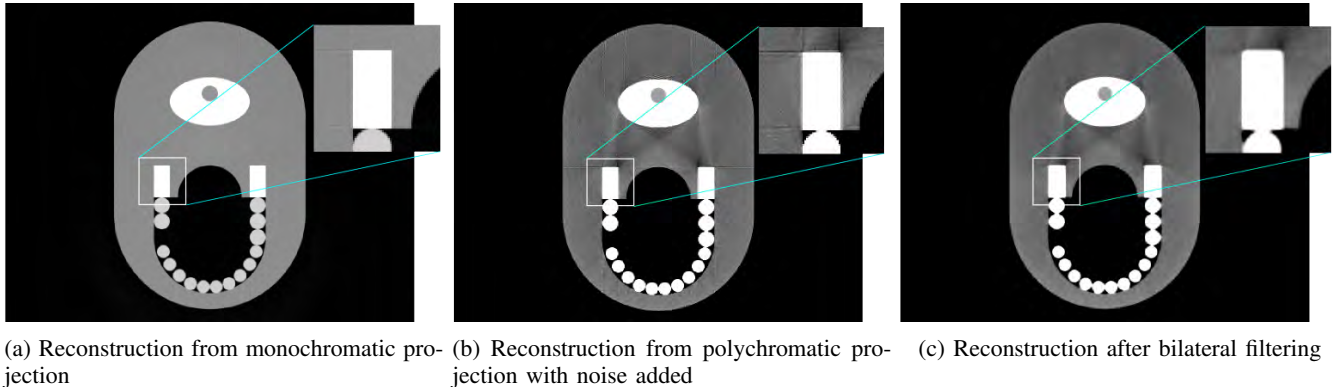


Fig. 2: Reconstruction results from simulated Forbild jaw phantom. Bilateral filtering:  $\sigma_D = 1mm$ ,  $5 \times 5$  neighborhood. L: 0.2; W: 0.2.

After bilateral filtering (Fig. 2c), the streak artifacts have been effectively suppressed. It has to be noticed that, in order to retain the spatial resolution, we did not apply a strong filter for smoothing. Because our main purpose on using bilateral filtering is keeping edge structural information for segmentation, and primary noise reduction. The reduction of strong streaks caused by bones and metal implants are the focus of artifact reduction.

Additive white Gaussian noise (AWGN) with different values of variance was used to simulate noisy images. Peak signal to noise ratio (PSNR) between original images and filtered images is used to measure the denoising performance of the bilateral filter.

$$PSNR = 20 \log \frac{\text{Peak Value}}{\sqrt{\frac{1}{MN} \sum_{y=1}^M \sum_{x=1}^N (\tilde{f}(x, y) - f(x, y))^2}} \quad (7)$$

### B. Edge Detection and Segmentation

In order to show the segmentation improvement benefiting from the edge-preserving filter, a hip prosthesis phantom (Fig. 3) and a real CT scanned dataset (Fig. 4) consisting of polyester, aluminum, steel and copper were evaluated.

Fig. 3 shows the segmentation and reconstruction results with 5mAs and 150mAs, respectively. It can be seen that, when the dose of radiation is increased, the reconstruction suffers less from noise. However, lower mAs levels are always desired due to dose considerations. Increased noise in reconstruction also affects segmentation. From the color-coded segmentation results, the original segmentation suffers from artifacts and noise. However, after applying the proposed method, the segmentation by K-means clustering improved.

In Fig. 4, strong dark and bright streak artifacts can be observed in the original reconstruction (Fig. 4a). Segmentation faces a big challenge created by similar dense objects' gray values overlapping in histogram and by streak distortions. Fig. 4c shows the color-coded segmentation result indicating four materials. It can be seen that large amounts of streaks are classified into materials, and the segmentation could not distinguish steel and copper because of their similar densities. This

poor initial segmentation will result in more computational effort in later artifact reduction. However, after we applied the material edge information (Fig. 4b) between reconstructions with and without bilateral filtering, the segmentation shows significant improvements (Fig. 4d). Table II lists the PSNR value for the hip prosthesis and the jaw phantom with AWGN applied in projection simulation with different values of variance. The Mean Square Error (MSE) is calculated to quantify

PSNR \ AWGN	0.1	0.2	0.3	0.4	0.5	0.6	0.7	0.8	0.9	1.0
Hip Phantom	38.69	37.18	36.04	35.39	34.56	32.50	30.34	29.32	28.37	27.52
Jaw Phantom	32.76	32.34	32.20	31.32	30.31	28.60	27.78	25.99	24.70	22.44

TABLE II: PSNR values of hip prosthesis phantom and jaw phantom with different AWGN variance values applied.

the misclassified voxels in segmentation image  $\tilde{\varphi}(x, y)$  and the ground truth  $\varphi(x, y)$ :

$$MSE = \frac{1}{XY} \sum_X \sum_Y [\varphi(x, y) - \tilde{\varphi}(x, y)]^2. \quad (8)$$

For the hip prosthesis phantom, the MSE value from original segmentation  $\varphi(x, y)$  is 11.16, and with the proposed bilateral filter applied  $\tilde{\varphi}(x, y)$  is 3.45. For the jaw phantom,  $\varphi(x, y)$  and  $\tilde{\varphi}(x, y)$  are 9.07 and 1.23, respectively.

## IV. CONCLUSION

In this paper, we used a nonlinear edge preserving bilateral filter as post-processing step for CT images containing dense materials. By applying the traditional bilateral filter on the original FDK reconstruction for noise reduction, and a modified bilateral edge detector for material structural information, the segmentation was able to return more accurate results, which significantly improved multi-material beam hardening and metal artifacts reduction. Evaluation results on simulated and real phantom data show noise reduction and significant improvement of segmentation, which can provide much faster convergence on later artifact reduction.

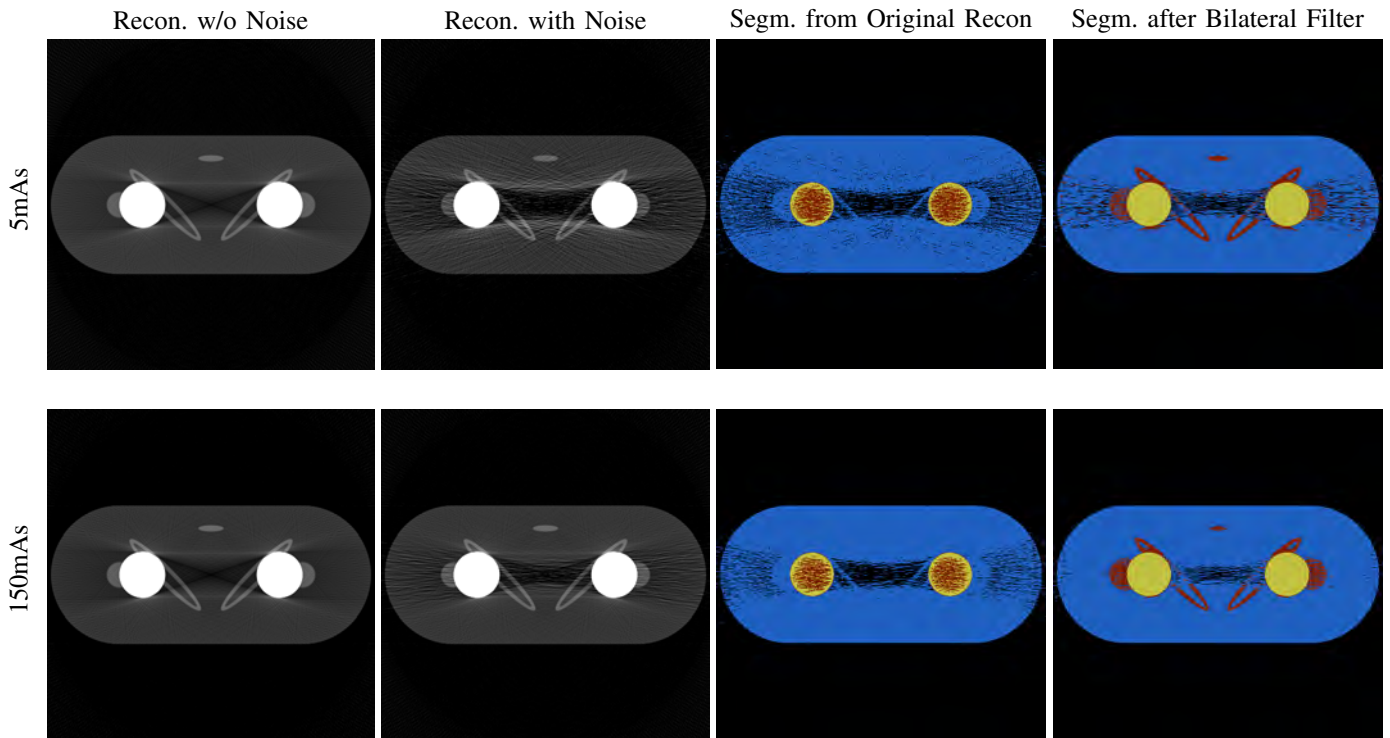
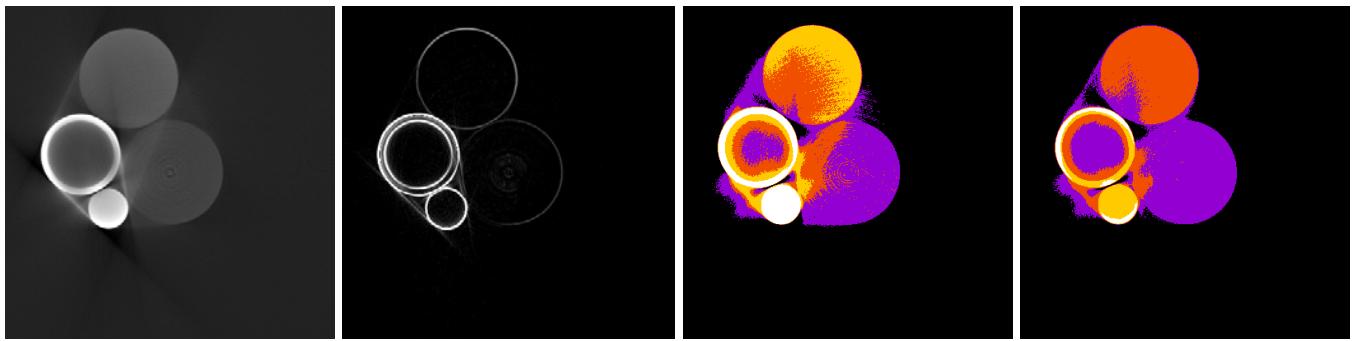


Fig. 3: Reconstruction and segmentation results of hip prosthesis phantom. 5mAs and 150mAs radiation levels were used for different noise levels. Original and segmentation with proposed method applied are displayed. L: 0.14; W: 0.22.



(a) Original reconstruction (b) Detected edge image using proposed bilateral edge detector (c) Color-coded segmentation result using K-means clustering (d) Color-coded segmentation result using K-means clustering with edge information

Fig. 4: Real CT dataset containing four materials. Results show original reconstruction image, difference image between the reconstruction with and without bilateral filtering applied, and segmentations with color-coded material identification. In ideal case: white–copper; yellow–iron; red–aluminum; purple–polyester. L: 0.11; W: 0.3.

#### ACKNOWLEDGMENT

The authors gratefully acknowledge funding of the Erlangen Graduate School in Advanced Optical Technologies (SAOT) by the German Research Foundation (DFG) in the framework of the German excellence initiative and the Erlangen Graduate School Heterogeneous Imaging Systems.

**Disclaimer:** The concepts and information presented in this paper are based on research and are not commercially available.

#### REFERENCES

- [1] G. Herman, "Correction for beam hardening in computed tomography," *Physics in Medicine and Biology*, vol. 24, p. 81, 1979.
- [2] J. Hsieh, R. C. Molthen, C. A. Dawson, and R. H. Johnson, "An iterative approach to the beam hardening correction in cone beam ct," *Medical Physics*, vol. 27, no. 1, pp. 23–29, 2000.
- [3] B. de Man, J. Nuyts, P. Dupont, G. Marchal, and P. Suetens, "An iterative maximum-likelihood polychromatic algorithm for ct," *IEEE Trans. Med. Imaging*, vol. 20, no. 10, pp. 999–1008, 2001.
- [4] I. Elbakri and J. Fessler, "Segmentation-free statistical image reconstruction for polyenergetic x-ray computed tomography with experimental validation," *Physics in Medicine and Biology*, vol. 48, p. 2453, 2003.

- [5] M. Kachelrieß and W. Kalender, "Improving pet/ct attenuation correction with iterative ct beam hardening correction," in *Nuclear Science Symposium Conference Record (NSS/MIC)*, vol. 4, 2005.
- [6] H. Gao, L. Zhang, Z. Chen, Y. Xing, and S. Li, "Beam hardening correction for middle-energy industrial computerized tomography," *Nuclear Science, IEEE Transactions on*, vol. 53, no. 5, p. 27962807, 2006.
- [7] M. Krumm, S. Kasperl, and M. Franz, "Reducing non-linear artifacts of multi-material objects in industrial 3d computed tomography," *NDT & E International*, vol. Vol 41, No 4, p. pp 242251, 2008.
- [8] G. V. Gompel, K. V. Slambrouck, M. Defrise, K. J. Batenburg, J. de Mey, J. Sijbers, and J. Nuyts, "Iterative correction of beam hardening artifacts in CT," *Medical Physics*, vol. 38, no. S1, pp. S36–S49, 2011.
- [9] Q. Yang, N. Maass, M. Tian, M. Elter, I. Schasiepen, A. Maier, and J. Hornegger, "Multi-material beam hardening correction (mmbhc) in computed tomography," in *Proc. Intl. Mtg. on Fully 3D Image Recon. in Rad. and Nuc. Med*, 2013, pp. 533–536.
- [10] C. Tomasi and R. Manduchi, "Bilateral filtering for gray and color images," in *Computer Vision, 1998. Sixth International Conference on*, 1998, pp. 839–846.
- [11] J. Giraldo, Z. Kelm, L. Guimaraes, L. Yu, J. Fletcher, B. Erickson, and C. McCollough, "Comparative study of two image space noise reduction methods for computed tomography: Bilateral filter and nonlocal means," 2009, pp. 3529–3532.
- [12] M. Tian, Q. Yang, A. Maier, I. Schasiepen, N. Maass, and M. Elter, "An automatic histogram-based initializing algorithm for k-means clustering in ct."
- [13] <http://www.imp.uni-erlangen.de/phantoms/hip/hipphantom.html>.
- [14] L. A. Feldkamp, L. C. Davis, and J. W. Kress, "Practical cone-beam algorithm," *Journal of the Optical Society of America*, vol. 1, pp. 612–619, 1984.